Theory of a collective atomic recoil laser

H. Y. Ling
Department of Chemistry and Physics, Rowan University, Glassboro, New Jersey 08028

H. Pu
Optical Science Center, The University of Arizona, Tucson, Arizona 85721

L. Baksmaty and N. P. Bigelow
Department of Physics and Astronomy and Laboratory for Laser Energetics, The University of Rochester, Rochester, New York 14627
(Received 7 September 2000; published 17 April 2001)

We perform a study of a collective atomic recoil laser (CARL) that goes beyond the initial growth period. The study is based on a theory that treats both internal and external degrees of atomic freedom quantum mechanically but regards the laser light as a classical field obeying Maxwell's equations. We introduce the concepts of momentum families and diffraction groups and organize the matter wave equations in terms of diffraction groups. The steady-state lasing conditions are discussed in connection with the probe gain in the recoil-induced resonances. The nontrivial steady states and the linear stability analysis of the steady states are both carried out by the method of two-dimensional continued fractions. Both stable and unstable nontrivial steady states are calculated and discussed in the context of regarding the CARL as multiwave mixing involving many modes of matter waves and two optical fields.

DOI: 10.1103/PhysRevA.63.053810 PACS number(s): 42.55.−f, 42.50.Vk, 32.80.Pj

I. INTRODUCTION

The collective atomic recoil laser (CARL) was proposed and studied by Bonifacio and collaborators [1–5] as an atomic analog of the free electron laser. In the Bonifacio model, two-level atoms are subject to two counterpropagating fields: a pump field from an external source and a spontaneously generated CARL signal (probe field) supported by a ring cavity. Essential to the CARL operation is the positive feedback between the probe signal and the atomic density grating, resulting from the modulation of the standing wave created by the probe and pump fields. An increased probe field can increase the amplitude of the standing wave and thereby enhance the strength of the atomic density grating; the enhanced atomic density grating, in turn, can backscatter the pump field more effectively off the grating into the probe field. These two processes go hand in hand, much like their counterparts in the free-electron laser, leading to a runaway amplification of the probe field. Experimental efforts have been made by Lippi *et al.* [6] and by Hemmer *et al.* [7], but the physical origin of the probe gain observed in the hot atoms by these two groups, and, in particular, its connection with the CARL mechanism, have remained controversial [8].

Earlier, Guo *et al.* [9,10] studied recoil-induced resonance (RIR) under the same atom-field configuration but without the ring cavity. A probe gain was found when the probe is tuned on the red side of the pump frequency and was later observed experimentally by Courtois *et al.* [11]. This gain was attributed to momentum redistribution among atoms of different momentum subgroups and could essentially be accounted for by the Raman transitions between different momentum states. Since a state in momentum space corresponds to a plane wave in position space, the population buildup of a particular momentum state is equivalent to the growth of the corresponding matter wave, which, in return, enhances the atomic density grating through its interference with the opposing wave. Thus, both the CARL and RIR should share the same gain mechanism as pointed out by Berman [12].

CARL theories can be broadly divided into semiclassical and quantum-mechanical ones, depending on how the center-of-mass motion is treated. The CARL theory of Bonifacio *et al.* [1–5] was developed by casting the Heisenberg equations into the *c*-number form for the expectation values of the relevant operators. This approach is semiclassical since the evolution of atomic momentum and position essentially follows Newton's second law. This approximation holds as long as $\Delta p_D \gg \hbar k$, where $\hbar k$ is the momentum of a single photon, and Δp_D is the width of the Gaussian momentum distribution. For atoms with $\Delta p_D \leqslant \hbar k$, the de Broglie matter wavelength exceeds that of the field and atoms can no longer be considered as localized classical particles moving under the influence of the electromagnetic fields. One must then seek a quantum-mechanical approach in which the center-of-mass motion is also treated quantum mechanically. This is precisely the method used by Moore and Meystre [13] to address the matter wave aspect of the CARL operation and by Berman [12] to make a comparison between RIR and the CARL.

In this paper, we perform a comprehensive study that goes beyond the initial period of growth for a CARL model consisting of ultracold atoms and far-off-resonant fields. The goal is to make the CARL theory nearly as comprehensive as its counterpart in a conventional laser system. The steady state in ordinary lasers is achieved by constantly pumping the atoms to the excited levels. Here, we seek to achieve steady state by a ''pump'' mechanism that maintains a steady flow of cold atoms into and out of the interaction region. The pump mechanism is simulated by a decay rate $\gamma_{||}$ whose inverse can be viewed as a transient interaction time

[9,10,14,15] and by a source containing a statistical mixture of ground state atoms. (For simplicity, we ignore the atom-atom collisions [16,17] by assuming that the atomic sample is sufficiently dilute.)

This paper will also explore the connection of the CARL with atom optics, an area of research focusing on how to manipulate matter waves by optical means. Much of the recent interest in the CARL has motivated largely by two factors. First, the recent experimental demonstrations of four-wave mixing [18,19] and superradiant Rayleigh scattering [20] have, to some degree, connections with the CARL mechanism [21]. Second, the CARL model can be viewed, from the perspective of atom optics, as a parametric amplifier [22,23] for the momentum side modes. This point of view has largely been explored along the line of how to control the quantum-statistical properties of side modes via optical fields [23,24]. In contrast, we focus on both the steady-state and dynamical behavior of the side modes.

It must be acknowledged that solving for the steady states is by no means trivial. First, the quantization of the center-of-mass momentum implies that a single internal energy level now becomes a momentum continuum. Second, in this system, a photon of one direction can be transferred into a photon of opposite direction by the Raman process involving the momentum states of the same internal level. Such a process can cause an infinite number of momentum states to be coupled. Finally, the fact that the loaded atoms are in a statistical mixture forces us to adopt the density matrix formalism as our theoretical framework. This introduces a further complication since each density matrix element is a function of two independent momenta.

In this paper, we make several conceptual advances to overcome these obstacles. First, we adapt the concept of momentum family from early studies in both two- [15,25] and three-level systems [26,27] to the CARL model. A momentum family is defined as consisting of all the states that are coupled under the coherent interaction. By dividing the total momentum space into different momentum families, we can concentrate on solution of the coupled equations involving the same family, whose dimension is typically much smaller than that of the total space. Next, we divide each momentum family into different diffraction groups that are coupled only to their immediate neighbors. This lends itself very nicely to the method of two-dimensional matrix continued fractions (2D MCF), developed by Cai *et al.* [28] (see also Pu *et al.* [29]) as a powerful tool for studying 2D laser cooling in a semi-classical approach. The advantage of this technique is evident from the standpoint of computational efficiency since the size of matrices to be inverted in the 2D MCF is limited by the size of the diffraction groups, which is much smaller than the size of the momentum family, and is, of course, much smaller than the size of the total space.

In Sec. II, we derive the atomic equations of motion in a way similar to that adopted by Moore and Meystre [13] and the field equations starting from Maxwell's equation following Berman [12]. However, the emphasis of the section is on the conceptual development of momentum families and diffraction groups. In Sec. III, we present the steady-state equations and linearized equations around steady states. This section also covers the numerical approach based on the 2D MCF for determining the steady states and their stabilities. In Sec. IV, we present and discuss the numerical results along with their implications. We show, from the consideration of the lasing condition, that RIR and the CARL share the same gain mechanism. In addition to the growth of the probe field, we also discuss the growth of the momentum side modes of the matter waves from the perspective of atom optics. The dynamics, including the instabilities, of the CARL signal will also be discussed. The main results are summarized in Sec. V.

II. THEORETICAL MODEL AND EQUATIONS OF MOTION

We consider a CARL system comprised of a CARL signal supported by a unidirectional ring cavity, a strong pump field directed almost opposite to the probe field, and a steady flow of an ultracold atomic beam into and out of the active region along a direction normal to the propagation of the fields. The atomic beam is made of two-level atoms with transition frequency Ω_{21}. The pump field features an amplitude F_2, a frequency ω_2, and a wave number $-k_2$, while the weak probe field is characterized by an amplitude F_1, a frequency ω_1, and a wave number k_1. The frequency ω_2 is fixed by the external source while ω_1, although close to the cavity mode frequency ω_C, is determined eventually by the steady-state condition. Furthermore, $k_2=\omega_2/c$, where c is the speed of light in vacuum, but $k_1=\omega_C/c$, since the probe is a cavity field.

A. Equations for the atomic variables

We begin by expanding the total field in terms of its components as

$$\hat{F}=\left(\frac{1}{2}F_1e^{-i\omega_2t+ik_1\hat{z}}+\frac{1}{2}F_2e^{-i\omega_2t-ik_2\hat{z}}\right)+\text{H.c.}, \qquad (1)$$

where the atomic center-of-mass position is treated as an operator $\hat{z}$ in anticipation of its interaction with ultracold atoms. Note that the field 1 is expanded in terms of ω_2 instead of ω_C or ω_1 merely for the purpose of making the derivation simple. We can do this here because ω_2, ω_C, and ω_1 are so close to each other that the assumption of F_1 being a slowly varying amplitude remains valid under the expansion (1). As in our earlier work [30,31], we choose to work in the Hilbert space spanned by $|i,p\rangle$, where i is the index of the internal energy and p is the eigenvalue of the z component of the center-of-mass momentum operator. (We restrict ourselves to a one-dimensional problem along z; a trace over x and y dimensions is implied wherever appropriate.) In this space, the atomic Hamiltonian

$$\hat{H}_A=\sum_{i=1,2}\int\left(\hbar\Omega_{21}\delta_{i,2}+\frac{p^2}{2m}\right)|i,p\rangle\langle p,i|dp \qquad (2)$$

is diagonal while the laser-atom interaction Hamiltonian $\hat{H}_{L\text{-}A}=-\hat{\mu}\hat{F}$, in the rotating wave approximation, takes the simple form

$$\hat{H}_{L\text{-}A}=-\hbar e^{-i\omega_2 t}\left[E_1\int |2,p+\hbar k_1\rangle\langle p,1|dp+E_2 \times\int |2,p-\hbar k_2\rangle\langle p,1|dp\right]+\text{H.c.}, \tag{3}$$

where

$$E_i=\frac{\mu_{21}F_i}{2\hbar}$$

is the Rabi frequency of the ith field and $\mu_{21}=\langle 2|\hat{\mu}|1\rangle$ is the atomic transition dipole moment. The evolution of the atomic density matrix operator ρ' in the Schrödinger picture obeys

$$\frac{d\rho'}{dt}=-\frac{i}{\hbar}[H,\rho']+\left(\frac{d\rho'}{dt}\right)_{inc}, \tag{4}$$

where $(d\rho'/dt)_{inc}$ is a shorthand notation for corrections associated with the finite transit time interaction and the random fluctuations due to spontaneous emission and collisions. We consider first the coherent part [the first term on the right hand side of Eq. (4)]. In terms of the slowly varying density matrix elements

$$\rho_{21}(p,p')\equiv\rho'_{21}(p,p')e^{i\omega_2 t},\qquad \rho_{11}(p,p')\equiv\rho'_{11}(p,p'), \tag{5}$$

we find that

$$\frac{d}{dt}\rho_{11}(p,p')=-i\left(\frac{p^2-p'^2}{2m\hbar}\right)\rho_{11}(p,p') +i[E_1^*\rho_{21}(p+\hbar k_1,p')-E_1\rho_{12}(p,p'+\hbar k_1)] +i[E_2^*\rho_{21}(p-\hbar k_2,p')-E_2\rho_{12}(p,p'-\hbar k_2)] \tag{6}$$

and

$$\frac{d}{dt}\rho_{21}(p,p')=-i\left(\frac{p^2-p'^2}{2m\hbar}-\Delta_A\right)\rho_{21}(p,p') +iE_1[\rho_{11}(p-\hbar k_1,p')-\rho_{22}(p,p'+\hbar k_1)] +iE_2[\rho_{11}(p+\hbar k_2,p')-\rho_{22}(p,p'-\hbar k_2)], \tag{7}$$

where

$$\Delta_A=\omega_2-\Omega_{21}$$

is the detuning of the pump relative to the atomic transition frequency. As stated in the Introduction, we are interested in the far-off-resonance case. This means that

$$|\Delta_A|\gg\Gamma,\gamma,|\omega_2-\omega_C|,\Delta\omega_D,$$

where Γ is the population decay rate of the excited level, γ the polarization dephasing rate, and $\Delta\omega_D$ the Doppler frequency width. Under this condition, we can ignore the excited population and solve for $\rho_{21}(p,p')$ from Eq. (7) in terms of the ground state density matrix elements

$$\rho_{21}(p,p')\approx-\frac{E_1}{\Delta_A}\rho_{11}(p-\hbar k_1,p')-\frac{E_2}{\Delta_A}\rho_{11}(p+\hbar k_2,p') \tag{8}$$

under the so-called adiabatic approximation. Substituting Eq. (8) into Eq. (6), we find that

$$\frac{d\rho_{11}(p,p')}{dt}=-i\left(\frac{p^2-p'^2}{2m\hbar}\right)\rho_{11}(p,p')-\gamma_{||} \times[\rho_{11}(p,p')-\rho_{11}^{(0)}(p,p')] +i\frac{E_2E_1^*}{\Delta_A}[\rho_{11}(p,p'-\hbar(k_1+k_2)) -\rho_{11}(p+\hbar(k_1+k_2),p')]+i\frac{E_2^*E_1}{\Delta_A} \times[\rho_{11}(p,p'+\hbar(k_1+k_2)) -\rho_{11}(p-\hbar(k_1+k_2),p')], \tag{9}$$

where the term associated with $\gamma_{||}$ is introduced phenomenologically to simulate the finite transit time process. Here the inverse of $\gamma_{||}$ is approximately with the interaction time resulting from atoms entering and leaving the interaction region, and

$$\rho_{11}^{(0)}(p,p')=2\pi\hbar L_z^{-1}W(p)\,\delta(p-p') \tag{10}$$

represents the momentum distribution of the loaded atomic sample with L_z being the effective interaction length along the z dimension and

$$\int_{-\infty}^{+\infty}W(p)dp=1.$$

Equation (10) corresponds to a Wigner function consisting of a momentum distribution times a uniform spatial density [12]. Since the atomic beam is assumed to be normal to the optical axis, we estimate $\gamma_{||}$ as the ratio of the diameter of the pump field to the mean longitudinal speed, and approximate $W(p)$ as the transverse momentum distribution.

B. Momentum families and diffraction groups

The idea of dividing the total momentum space into different families emerged in the study of the momentum distribution of two-level atoms interacting with a near-resonant

standing wave [15,25]. This approach gained popularity and was, in fact, instrumental in the analysis of subrecoil laser cooling for three-level systems [26,27]. To be specific, consider a situation in which two counterpropagating fields with the same wave number k interact independently with the two transitions in a degenerate Λ atomic system. Let $|3,p\rangle$ represent the excited momentum state while $|1,p\rangle$ and $|2,p\rangle$ stand, respectively, for the momentum states of the two degenerate ground levels. With an appropriate choice of the field polarizations, we can assume, without loss of generality, that the forward field interacts with the $|3\rangle \leftrightarrow |1\rangle$ transition while the backward field is coupled to the $|3\rangle \leftrightarrow |2\rangle$ transition. Because of the momentum conservation, an atom in $|3,p\rangle$ can only make a transition to $|1,p-\hbar k\rangle$ ($|2,p+\hbar k\rangle$) by emission of a forward (backward) photon. Conversely, an atom in $|1,p-\hbar k\rangle$ ($|2,p+\hbar k\rangle$) can only be pumped to $|3,p\rangle$ by absorption of a forward (backward) photon. We are thus led to define a momentum family $F(p_0)$, where $-\infty \leqslant p_0 \leqslant +\infty$, to consisting of three members $\{|3,p_0\rangle, |1,p_0-\hbar k\rangle, |2,p_0+\hbar k\rangle\}$, that can only recycle among themselves under the coherent interaction.

In our model, the momentum exchange between photons and atoms is accomplished by a Raman anti-Stokes process mediated by the effective two-photon field $|E_1 E_2^*/\Delta_A|$. An atom in $|1,p\rangle$ can make a transition to $|1,p+\hbar(k_1+k_2)\rangle$ by simultaneous absorption of a CARL photon and emission of a pump photon. Conversely, an atom in $|1,p\rangle$ can make a transition to $|1,p-\hbar(k_1+k_2)\rangle$ by simultaneous emission of a CARL photon and absorption of a pump photon. In this way, an atom initially prepared in $|1,p\rangle$ can end up in $|1,p+n\hbar(k_1+k_2)\rangle$, where $-\infty \leqslant n \leqslant \infty$, by n such Raman transitions. Based on this discussion, we define a momentum family $F(p_0)$, where $0 \leqslant p_0 < \hbar(k_1+k_2)$, to be comprised of all the base states $\{|1,p_0+n\hbar(k_1+k_2)\rangle, -\infty \leqslant n \leqslant \infty\}$. We limit p_0 to the values between 0 and $\hbar(k_1+k_2)$ for the purpose of uniqueness because if, for example, $p_0 > \hbar(k_1+k_2)$ but less than $2\hbar(k_1+k_2)$, the element $|1,p_0+n\hbar(k_1+k_2)\rangle$ should, in fact, belong to $F(p_0')$ where $p_0' = p_0 - \hbar(k_1+k_2) < \hbar(k_1+k_2)$. Clearly, if an atom starts from a base state belonging to a family $F(p_0)$ it can only recycle among the states of the same family under the Raman process. Indeed, spontaneous emission can cause atoms to move from one family to another due to the random momentum exchange in the process of spontaneous emission. However, this is of no concern here because spontaneous emission is absent from our model.

As noted in the Introduction, the injected atoms are in a state that is best described by the density matrix formalism. A density matrix element $\rho_{11}(p_0+n\hbar(k_1+k_2), p_0'+m\hbar(k_1+k_2))$ can be formed by members from two different families if $p_0 \neq p_0'$. However, because the injected atoms are assumed to be spatially uniform, they lack the coherences between the members of different families. Hence, the elements $\rho_{11}(p_0+n\hbar(k_1+k_2), p_0'+m\hbar(k_1+k_2))$ in which $p_0 \neq p_0'$ cannot become different from zero in the course of the evolution. We then need to consider only the density matrix elements formed by members of the same family $p_0 = p_0'$. In a typical numerical calculation, we must define cutoff momenta $P_{\max}$ and $P_{\min}$ in order to close each momentum family. In addition, we need to divide $0 \leqslant p_0 \leqslant \hbar(k_1+k_2)$ into L subintervals so that there is a total number of L momentum families. (In contrast, in three-level systems, the momentum family is closed by itself but p_0 is truncated according to the relevant momentum space.) At this point, we associate each momentum family with a map of a square lattice of length $\hbar(k_1+k_2)$ in a two-dimensional momentum space as shown in Fig. 1. Situated on a lattice site of coordinate (n,m) is the density matrix element $\rho_{11}(p,p')$, where $p = p_0 + n\hbar(k_1+k_2)$ and $p' = p_0 + m\hbar(k_1+k_2)$. The map for $F(p_0+\Delta p_0)$ can be produced by shifting the $F(p_0)$ map along the $+45°$ direction by a displacement of $\sqrt{2}\Delta p_0$. It is then not difficult to visualize that as p_0 changes from 0 to $\hbar(k_1+k_2)$ the momentum space will be filled with density matrix elements along all the $+45°$ lines as shown in Fig. 2. This pattern suggests that we introduce the following expansion

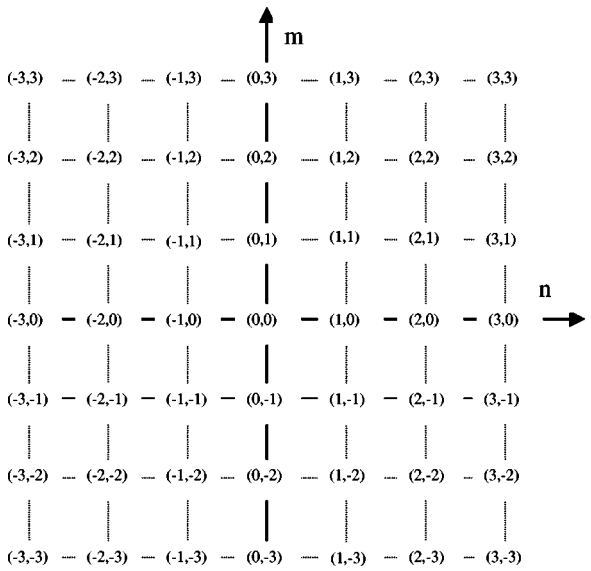

FIG. 1. A map of the density matrix elements of a single momentum family with $N_{\max}=3$. The cutoff momenta for a momentum family $F(p_0)$ are defined as $P_{\min}=p_0-N_{\max}$ and $P_{\max}=p_0+N_{\max}$ in units of $\hbar(k_1+k_2)$.

$$\rho_{11}(p,p') = 2\pi\hbar L_z^{-1} \sum_{l=-\infty}^{+\infty} R_l(p)\,\delta(p-p'-l\hbar(k_1+k_2)), \tag{11}$$

where the Dirac δ function serves as a constraint, limiting all the elements to the $+45°$ diagonal lines. At this point, we define the lth diffraction group as consisting of all the elements $\rho_{11}(p,p')$ in which $p-p'-l\hbar(k_1+k_2)=0$. The name of ''diffraction group'' can be easily understood once we transform the matrix element $\rho_{11}(p,p')$ into the z representation

$$\langle z,1|\rho|1,z\rangle = \frac{1}{2\pi\hbar}\int\int \rho_{11}(p,p')e^{i(p-p')z/\hbar}dpdp', \tag{12}$$

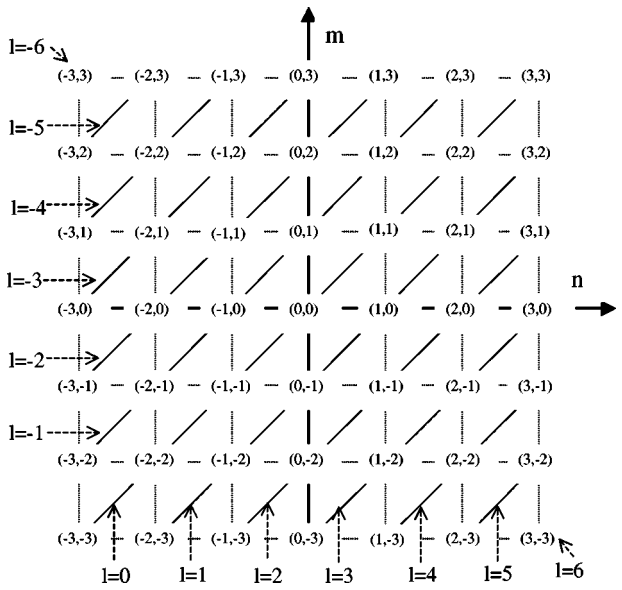

FIG. 2. A map of diffraction groups with $N_{\max}=3$. Note that $l_{\max}=-l_{\min}=2N_{\max}=6$, where $l_{\max}$ and $l_{\min}$ are, respectively, the highest and lowest diffraction group numbers.

which, with the help of Eq. (11), can also be written in the form

$$\langle z,1|\rho|1,z\rangle = L_z^{-1}\sum_l e^{il(k_1+k_2)z}\int R_l(p)dp. \tag{13}$$

In an atomic diffraction experiment in which the incident atomic beam is normal to the z direction, the atomic beam will be diffracted into different angles corresponding to different values of l with a weight proportional to $\int R_l(p)dp$. The functions $R_l(p)$ satisfy two important relations: first,

$$\int R_0(p)dp = 1, \tag{14}$$

which represents the population conservation and can be derived from Eqs. (9), (10), and (11) [or later directly from Eq. (28)]; second,

$$R_{-l}(p) = R_l(p + l\hbar(k_1+k_2))^*, \tag{15}$$

due to the fact that $\rho_{ij}(p,p') = \rho_{ji}(p',p)^*$. The concept of the momentum family combined with the concept of the diffraction group establishes the conceptual framework for an efficient numerical approach to the steady-state problem.

C. Equations for the fields

We now turn our attention to the evolution of the fields, starting from Maxwell's equation for the total field

$$\frac{\partial^2 F}{\partial z^2} - \frac{1}{c^2}\frac{\partial^2 F}{\partial t^2} = \mu_0 \frac{\partial^2 P}{\partial t^2},$$

where P is the macroscopic atomic polarization. A field of the form given by Eq. (1) can only be driven by a polarization of similar form:

$$P = \left(\frac{1}{2}P_1 e^{-i\omega_2 t + ik_1 z} + \frac{1}{2}P_2 e^{-i\omega_2 t - ik_2 z}\right) + \text{c.c.}, \tag{16}$$

where P_i $(i=1,2)$ are slowly varying amplitudes. Note that we have changed $\hat{z}$ into z because we consider Maxwell's equation as an average equation in $|z\rangle$ space. Under the slowly varying amplitude approximation, we find

$$\frac{\partial E_i}{\partial t} + c\frac{\partial E_i}{\partial z} = i\frac{\omega_2 \mu_{21}}{4\varepsilon_0 \hbar}P_i - i\left[k_i^2 - \left(\frac{\omega_2}{c}\right)^2\right]\frac{c^2}{2\omega_2}E_i. \tag{17}$$

The polarization, on the other hand, is an average variable in the position z, and is calculated through the trace over the internal degrees of freedom. These considerations lead to

$$P = N\mu_{21}L_z\langle z,2|\rho'|1,z\rangle + \text{c.c.}, \tag{18}$$

where N is the atomic density. $\langle z,2|\rho'|1,z\rangle$ is linked to the density matrix element in momentum space by the transformation

$$\langle z,2|\rho'|1,z\rangle = \frac{1}{2\pi\hbar}\int\int \rho'_{21}(p,p')e^{i(p-p')z/\hbar}dpdp', \tag{19}$$

which becomes

$$\langle z,2|\rho'|1,z\rangle = \frac{1}{2\pi\hbar}e^{-i\omega_2 t}\int\int \rho_{21}(p,p')e^{i(p-p')z/\hbar}dpdp' \tag{20}$$

after Eq. (5) is taken into account. We use Eqs. (8) and (11) to express $\rho_{21}(p,p')$ in terms of the diffraction groups,

$$\begin{aligned}\rho_{21}(p,p') = &-2\pi\hbar L_z^{-1}\frac{E_1}{\Delta_A}\sum_{l=-\infty}^{\infty} R_l(p-\hbar k_1)\\ &\times\delta(p-\hbar k_1 - p' - l\hbar(k_1+k_2))\\ &-2\pi\hbar L_z^{-1}\frac{E_2}{\Delta_A}\sum_{l=-\infty}^{\infty} R_l(p+\hbar k_2)\\ &\times\delta(p+\hbar k_2 - p' - l\hbar(k_1+k_2)).\end{aligned} \tag{21}$$

In order to yield the polarization in the form of Eq. (16), we only have to retain terms proportional to $\delta(p-p'-\hbar k_1)$ and $\delta(p-p'+\hbar k_2)$. This means that we keep terms with $l=0$ and $l=-1$ in the first sum and the terms with $l=0$ and $l=1$ in the second sum of Eq. (21). This leads to

$$\rho_{21}(p,p') = -2\pi\hbar L_z^{-1}\left[\frac{E_1}{\Delta_A}R_0(p-\hbar k_1) + \frac{E_2}{\Delta_A}R_{+1}(p+\hbar k_2)\right]\delta(p-p'-\hbar k_1) - 2\pi\hbar L_z^{-1}\left[\frac{E_2}{\Delta_A}R_0(p+\hbar k_2) + \frac{E_1}{\Delta_A}R_{-1}(p-\hbar k_1)\right]\delta(p-p'+\hbar k_2). \quad (22)$$

By combining Eqs. (16), (18), (20), and (22), we find

$$P_1 = -\frac{2N\mu_{21}}{\Delta_A}\left[E_1 + E_2\int R_{+1}(p)dp\right], \quad (23)$$

$$P_2 = -\frac{2N\mu_{21}}{\Delta_A}\left[E_2 + E_1\int R_{-1}(p)dp\right], \quad (24)$$

where Eq. (14) has been used. Inserting Eqs. (23) and (24) into Eqs. (17), we turn Eqs. (17) into

$$\frac{\partial E_2}{\partial t} + c\frac{\partial E_2}{\partial z} = -i\frac{N\mu_{21}^2\omega_2}{2\hbar\varepsilon_0\Delta_A}E_1\int R_{-1}(p)dp, \quad (25)$$

$$\frac{\partial E_1}{\partial t} + c\frac{\partial E_1}{\partial z} = i\delta_C E_1 - i\frac{N\mu_{21}^2\omega_2}{2\hbar\varepsilon_0\Delta_A}E_2\int R_{+}(p)dp, \quad (26)$$

where

$$\delta_C = \omega_2 - \omega_C.$$

In reaching Eqs. (25) and (26), we have ignored the term $-iN\mu_{21}^2\omega_2 E_i/2\hbar\varepsilon_0\Delta_A$ from both equations since it represents a constant frequency shift, and dropping it amounts to an adjustment of the pump frequency ω_2 by a constant and will therefore not affect the dynamics of the fields. Further, in reaching Eq. (26), we used the approximation $\omega_2+\omega_C \approx 2\omega_2$. At this point, we assume that E_2 is much stronger than E_1 and its depletion is ignored. This allows us to treat E_2 as a constant. Finally, we substitute the space derivative $\partial E_1/\partial z$ of Eq. (26) by $\kappa E_1/c$ and N by a mean atomic density $n = NLz/\Lambda$ as a means to simulate the result under the mean field limit [5,32]

$$\frac{dE_1}{dt} = i\delta_C E_1 - i\frac{n\mu_{21}^2\omega_2}{2\hbar\varepsilon_0\Delta_A}E_2\int R_{+}(p)dp - \kappa E_1, \quad (27)$$

where $\kappa = c\,|\ln R|/\Lambda$, R is the power reflectivity of both input and output couplers, and Λ is the total length of the ring cavity; in the mean field limit the effect of output couplers and the free portion of the cavity on the dynamics of the cavity field can be taken care of in a self-consistent manner.

D. A summary of the basic equations in scaled form

We define a unit system in which $\hbar(k_1+k_2)$ is the unit of momentum, $1/\omega_{2r}$ the unit of time, and ω_{2r} the unit of any frequencies and decay rates, where

$$\omega_{2r} = \hbar\frac{(k_1+k_2)^2}{2m}$$

is the two-photon recoil frequency shift. Equations for the diffraction group are derived, by inserting Eq. (11) into Eq. (9), with the result

$$\frac{dR_l(p)}{dt} = -il(2p-l)R_l(p) + iA^*[R_{l+1}(p) - R_{l+1}(p+1)] + iA[R_{l-1}(p) - R_{l-1}(p-1)] - \gamma_{||}[R_l(p) - W(p)\delta_{l,0}], \quad (28)$$

where A is a new field variable defined as

$$A = \frac{E_2^* E_1}{\Delta_A}.$$

The equation for A is derived from Eq. (27) as

$$\frac{dA}{dt} = i\delta_C A - i\alpha\int R_{+1}(p)dp - \kappa A, \quad (29)$$

where

$$\alpha = \frac{n\mu_{21}^2\omega_2|E_2|^2}{2\hbar\varepsilon_0\omega_{2r}^2\Delta_A^2}.$$

Note that the same notations are used for the scaled variables for simplicity. These equations, in the absence of the terms associated with κ and $\gamma_{||}$, are formally equivalent to those obtained by Moore and Meystre [13].

III. STEADY STATES AND STABILITY ANALYSIS

A. The trivial steady state and collective instabilities

The trivial steady state

$$A^{st} = 0,$$

$$R_l^{st}(p) = W(p)\delta_{l,0}$$

is found by inspection of Eqs. (28) and (29) at steady state. By linearizing Eqs. (28) and (29) around the trivial steady state, we find

$$\frac{d\delta R_{+1}(p)}{dt} = -i(2p-1)\delta R_{+1}(p) + i\delta A[W(p) - W(p-1)] - \gamma_{||}\delta R_{+}(p), \quad (30)$$

$$\frac{d\delta A}{dt} = i\delta_C\delta A - i\alpha\int \delta R_{+1}(p)dp - \kappa\delta A, \quad (31)$$

where both δA and $\delta R_l(p)$ represent infinitesimally small departures from the corresponding steady-state values. Introducing the following ansatz involving the eigenvalue λ:

$$\delta R_{+1}(p) \propto e^{\lambda t},$$

$$\delta A \propto e^{\lambda t},$$

we transform Eqs. (30) and (31) into

$$\delta R_{+1}(p) = i\,\delta A \frac{W(p) - W(p-1)}{\lambda + \gamma_{||} + i(2p-1)}, \tag{32}$$

$$\lambda\,\delta A = i\,\delta_C \delta A - i\,\alpha \int \delta R_{+1}(p)\,dp - \kappa\,\delta A. \tag{33}$$

Finally, by eliminating $\delta R_{+1}(p)$ from Eq. (33) with the help of Eq. (32), we arrive at the desired eigenvalue equation

$$f(\lambda) \equiv \lambda + \kappa - i\,\delta_C - \alpha \int \frac{W(p) - W(p-1)}{\lambda + \gamma_{||} + i(2p-1)}\,dp = 0. \tag{34}$$

The roots of $f(\lambda)=0$ are determined numerically and the emergence of any roots with positive real parts is an indicative of collective instabilities. For the positive roots, we follow Moore [13] and apply the Parseval relation of Fourier transformation to reduce Eq. (34) to

$$f(\lambda) = \lambda + \kappa - i\,\delta_C - \alpha\pi \int_0^\infty e^{-\omega^2 \Delta p_D^2/4 - \omega(\lambda + \gamma_{||})/2} \times (e^{i\omega/2} - e^{-i\omega/2})\,d\omega,$$

which, expressed in terms of error functions, becomes

$$f(\lambda) = \lambda + \kappa - i\,\delta_C + \frac{\alpha}{2}\frac{\sqrt{\pi}}{\Delta p_D} i \left[e^{(\lambda + \gamma_{||} - i)^2/4\Delta p_D^2} \mathrm{erfc}\left(\frac{1}{2}\frac{\lambda + \gamma_{||} - i}{\Delta p_D} \right) - e^{(\lambda + \gamma_{||} + i)^2/4\Delta p_D^2} \mathrm{erfc}\left(\frac{1}{2}\frac{\lambda + \gamma_{||} + i}{\Delta p_D} \right) \right]. \tag{35}$$

B. Nontrivial steady states

1. Equations

We now seek the nontrivial steady states that both the CARL signal and matter waves might be able to reach after a long period of time. (From now on, we call nontrivial steady states ''steady states'' for simplicity.) It is well known from conventional laser theory that the output laser will typically oscillate at a frequency different from the cavity mode frequency [33,32]. For this reason, we look for the steady-state CARL field in the form of

$$A(t) = |A^{st}| e^{-i\delta_L t + i\phi}, \tag{36}$$

where

$$\delta_L = \omega_1 - \omega_2 \tag{37}$$

is the laser frequency relative to the pump frequency and will be determined from the steady-state condition, and ϕ is an unknown arbitrary phase. Here, the laser frequency shift δ_L is measured with respect to the pump frequency not the cavity frequency because the field [Eq. (1)] is expanded around the pump frequency. As a consequence of the shift in the probe frequency, the matter waves are expected to experience similar frequency shifts. Indeed, we find, after Eq. (36) is inserted into Eqs. (28) and (29), that only if

$$R_l(p,t) = R_l^{st}(p) e^{il(-\delta_L t + \phi)} \tag{38}$$

can the time variable be explicitly eliminated. These considerations lead to the coupled nonlinear equations

$$i(\delta_C + \delta_L)|A^{st}| - i\,\alpha \int R_{+1}^{st}(p)\,dp - \kappa |A^{st}| = 0, \tag{39}$$

$$-\gamma_{||} W(p)\,\delta_{l,0} = -[il(2p - l - \delta_L) + \gamma_{||}] R_l^{st}(p) + i|A^{st}|[R_{l+1}^{st}(p) - R_{l+1}^{st}(p+1)] + i|A^{st}|[R_{l-1}^{st}(p) - R_{l-1}^{st}(p-1)], \tag{40}$$

whose roots correspond to the steady-state variables of our interest.

Next, in order to perform stability analysis of the steady states, we introduce, in terms of small perturbations δA, δA^*, and $\delta R_l(p)$, the following linearization scheme:

$$A(t) = |A^{st}| e^{-i\delta_L t + i\phi} + \delta A e^{-i\delta_L t + i\phi} e^{\lambda t}, \tag{41}$$

$$A^*(t) = |A^{st}| e^{i\delta_L t - i\phi} + \delta A^* e^{i\delta_L t - i\phi} e^{\lambda t}, \tag{42}$$

$$R_l(p,t) = R_l^{st}(p) e^{il(-\delta_L t + \phi)} + \delta R_l(p) e^{il(-\delta_L t + \phi)} e^{\lambda t}, \tag{43}$$

where λ is the eigenvalue. Substituting Eqs. (41) and (43) into Eqs. (28) and (29) and keeping terms linear with respect to δA, δA^*, and $\delta R_l(p)$, we arrive at the coupled linear equations

$$[i(\delta_L + \delta_C) - \kappa - \lambda]\delta A - i\,\alpha \int \delta R_{+1}(p)\,dp = 0, \tag{44}$$

$$[-i(\delta_L + \delta_C) - \kappa - \lambda]\delta A^* + i\,\alpha \int \delta R_{-1}(p)\,dp = 0, \tag{45}$$

$$-i\,\delta A[R_{l-1}^{st}(p) - R_{l-1}^{st}(p-1)] - i\,\delta A^* \times [R_{l+1}^{st}(p) - R_{l+1}^{st}(p+1)] = -[il(2p - l - \delta_L) + \gamma_{||} + \lambda]\delta R_l(p) + i|A^{st}| \times [\delta R_{l+1}(p) - \delta R_{l+1}(p+1)] + i|A^{st}| \times [\delta R_{l-1}(p) - \delta R_{l-1}(p-1)], \tag{46}$$

from which we can determine the eigenvalue λ.

2. Numerical method: Two-dimensional matrix continued fraction

The diffraction groups are coupled in much the same way as the N ''photon'' groups [28,29] are coupled. This can be seen from Eq. (40) where the lth diffraction group is coupled only to the $(l \pm 1)$th group. Naturally, we are led to build our numerical method upon the method 2D MCF. As an illustration, we construct a 2D MCF by which $R_l^{st}(p)$ can be obtained efficiently from Eq. (40), given a pair of $|A^{st}|$ and δ_L. A similar but more complex method is developed in Appendix A for determining eigenvalues from Eqs. (44), (45), and

(46). To begin with, we introduce, for a given momentum family p_0, a vector $\vec{S}_l$ of dimension $D(l)=2N_{\max}-l+1$, containing all the elements in the lth diffraction group, where $0\leqslant l\leqslant l_{\max}=2N_{\max}$. Here, we have truncated the momentum space at $p_0\pm N_{\max}$ so that a momentum family is closed with $2N_{\max}+1$ members, ranging from $|1,p_0-N_{\max}\rangle$ to $|1,p_0+N_{\max}\rangle$.. This approximation holds as long as the momentum states beyond $p_0\pm N_{\max}$ remain virtually intact at long time. In addition, we have limited l to positive values since the negative diffraction groups can be derived from the positive ones according to Eq. (15). Let $p[n]=p_0+l+n-N_{\max}-1$, where n is integer. $\vec{S}_l$ is defined according to

$$\vec{S}_l[n]=R_l^{st}(p[n]),\ n=1,2,\ldots,D(l).$$

In this definition, we have sought to place each element of the lth group into $\vec{S}_l$ in the sequence from the bottom left to the top right end along the $+45^\circ$ line of the lth group as shown in Fig. 2. Next, we introduce three matrices: $M_{l,l}$, $M^+_{l,l+1}$, and $M^-_{l,l-1}$. $M_{l,l}$ is a diagonal matrix of dimension $D(l)\times D(l)$ with its diagonal elements being defined as

$$M_{l,l}[n][n]=-il(2p[n]-l-\delta_L)-\gamma_{||}.$$

$M^+_{l,l+1}$ is a matrix of dimension $D(l)\times D(l+1)$. The elements of $M^+_{l,l+1}$ are all zero except those defined below:

$$M^+_{l,l+1}[n][n]=-i|A^{st}|,\ M^+_{l,l+1}[n+1][n]=i|A^{st}|.$$

$M^-_{l,l-1}$ is a matrix of dimension $D(l)\times D(l-1)$. The elements of $M^-_{l,l-1}$ are also all zero with the exception of

$$M^-_{l,l-1}[n][n]=-i|A^{st}|,\quad M^-_{l,l-1}[n][n+1]=i|A^{st}|.$$

The coupled matrix equations are written in terms of these definitions as

$$M_{l,l}\vec{S}_l+M^-_{l,l-1}\vec{S}_{l-1}+M^+_{l,l+1}\vec{S}_{l+1}=\vec{W}_0\delta_{l,0},\qquad(47)$$

where $\vec{W}_0$ is a vector of dimension $D(0)$ defined as

$$\vec{W}_0[n]=W(p[n]).$$

To solve Eq. (47), we introduce a forward ansatz for $l>0$,

$$\vec{S}_l=-Q^+_l M^-_{l,l-1}\vec{S}_{l-1},\qquad(48)$$

where Q^+_l is a square matrix of $D(l)\times D(l)$. Q^+_l is found, by replacing $\vec{S}_{l+1}$ in Eq. (47) with $-Q^+_{l+1}M^-_{l+1,l}\vec{S}_l$ [derived from Eq. (48)], to satisfy the recursive relation

$$Q^+_l=(M_{l,l}-M^+_{l,l+1}Q^+_{l+1}M^-_{l+1,l})^{-1}.\qquad(49)$$

Because of the momentum cutoff, the diffraction groups beyond $l=l_{\max}$ must all vanish. In particular, $\vec{S}_{l_{\max}+1}=0$. With this consideration, we find from Eq. (47) with $l=l_{\max}$ that $\vec{S}_{l_{\max}}=-(M_{l_{\max},l_{\max}})^{-1}M^-_{l_{\max},l_{\max}-1}\vec{S}_{l_{\max}-1}$, which, compared with Eq. (48), gives rise to

$$Q^+_{l_{\max}}=(M_{l_{\max},l_{\max}})^{-1}.\qquad(50)$$

Hence, all the matrices Q^+_l with $0<l<l_{\max}$ can be obtained from Eq. (49) recursively, starting from Eq. (50). For $l=0$, we have from Eq. (47) that

$$M_{0,0}\vec{S}_0+M^-_{0,-1}\vec{S}_{-1}+M^+_{0,+1}\vec{S}_1=\vec{W}_0.\qquad(51)$$

But since

$$\vec{S}_1=-Q^+_1M^-_{1,0}\vec{S}_0\qquad(52)$$

and $\vec{S}_{-1}=\vec{S}^*_1$ according to Eq. (15), we find from Eq. (51) that

$$\vec{S}_0=(M_{00}-M^+_{0,1}Q^+_1M^-_{1,0}-M^-_{0,-1}Q^{+*}M^{-*}_{1,0})^{-1}\vec{W}_0.$$

Once $\vec{S}_0$ is determined, we can solve for $\vec{S}_1$ from Eq. (52). The elements in $\vec{S}_1$ represent $R^{st}_{+1}(p)$ of a particular momentum family. In order to perform the integral in Eq. (39), we need to construct a complete set of $R^{st}_{+1}(p)$. This is done by repeating the same steps for all the momentum families. In summary, we have developed an algorithm that allows us to evaluate the left side of Eq. (39), given a pair of $|A^{st}|$ and δ_L. This algorithm together with a root searching program [34,35] will enable us to determine $|A^{st}|$, δ_L, and all the $R^{st}_l(p)$ simultaneously.

IV. DISCUSSION

A. Lasing conditions and collective instabilities of the trivial steady state

It is well known from conventional laser theory that lasing takes place when the linear gain exceeds the cavity loss. To study the lasing condition, we choose $|A^{st}|$ as the perturbation parameter and expand both $R^{st}_+(p)$ and δ_L perturbatively as

$$R^{st}_+(p)=R^{st(0)}_+(p)+R^{st(1)}_+(p)+\cdots,$$

$$\delta_L=\delta^{(0)}_L+\delta^{(1)}_L+\cdots.$$

We seek from Eq. (40) a solution correct to the first order in $|A^{st}|$,

$$R^{st(1)}_{+1}(p)=i|A^{st}|\frac{W(p)-W(p-1)}{\gamma_{||}+i(2p-1-\delta^{(0)}_L)},\qquad(53)$$

which, combined with Eq. (39), gives rise to the threshold condition

$$-i\delta^{(0)}_L-i\delta_C+\kappa-\alpha\int\frac{W(p)-W(p-1)}{\gamma_{||}+i(2p-1-\delta^{(0)}_L)}dp=0.\qquad(54)$$

Note that Eq. (54) is the same as Eq. (34) when $\lambda\equiv\lambda_r+i\lambda_i$ in Eq. (34) is substituted by $\lambda_r=0$ and $\lambda_i=-\delta^{(0)}_L$. This observation represents the simple fact that the steady

states that can grow from noise must start from unstable trivial steady states. Thus, steady-state lasings and collective instabilities share the same parameter space. To gain further insight, we organize the real part of Eq. (54) in the form

$$\gamma_{||}\int \frac{W(p+1/2)-W(p-1/2)}{\gamma_{||}^2+(2p-\delta_L^{(0)})^2}dp=\frac{\kappa}{\alpha}, \tag{55}$$

which simply means that the gain equals the loss at the threshold. However, the left side of Eq. (55) can now be identified as the probe absorption spectrum of RIR [9,10], contributed by the Raman transitions between $|1,p+1/2\rangle$ and $|1,p-1/2\rangle$ of different p. The dominant contributions to the spectrum must come from those Raman transitions whose p are around $p_R \equiv \delta_L^{(0)}/2$, where the two-photon resonance condition or equivalently the energy conservation law is satisfied. Note that here the momentum of the initial state $|1,p+1/2\rangle$ is greater than that of the final state $|1,p-1/2\rangle$ by one momentum unit (meaning k_1+k_2). Such a process, consistent with the momentum conservation law, must correspond to the simultaneous emission of a probe (forward) photon and absorption of a pump (backward) photon. Clearly, in order for the probe to be amplified, the population in the state $|1,p+1/2\rangle$ must exceed that in the state $|1,p-1/2\rangle$. If $\delta_L^{(0)}=0$, p_R will be zero; because $W(p)$ is symmetric with respect to $p=0$, the population of the negative momentum will balance that of the positive momentum. [Unless indicated otherwise, $W(p)$ is assumed to be a Gaussian distribution of momentum width Δp_D: $W(p)=e^{-(p/\Delta p_D)^2}/\sqrt{\pi}\Delta p_D$.] As a result, the probe field can be neither amplified nor absorbed when $\delta_L^{(0)}=0$. However, if $\delta_L^{(0)}<0$, p_R will be aligned in the negative momentum region where, by inspection of the atomic momentum distribution, the population at $p+1/2$ is always larger than that at $p-1/2$, that is, $W(p+1/2)-W(p-1/2)>0$, and vice versa if $\delta_L^{(0)}>0$ [10]. As a result, we expect that the probe absorption spectrum will change from gain to absorption as the probe is tuned from the red side to the blue side of the pump field as shown in Fig. 3. Thus, to produce the steady-state CARL field, $\delta_L^{(0)}$ must be negative. This discussion clearly demonstrates that both the RIR and CARL share the same gain mechanism. The difference is that $\delta_L^{(0)}$ is a preset value in the RIR but is fixed by the threshold condition in the CARL.

Since δ_C can be controlled externally in the CARL, we calculate the threshold value α as a function of δ_C for several Δp_D and plot the results in Fig. 4. Note that since α is directly proportional to the atomic density any discussions about α can be equally passed onto the atomic density. Figure 4 indicates that for a given Δp_D laser action takes place only when the CARL is operated at parameters above the corresponding boundary. It has several features that can all be accounted for by the spectroscopic features presented in Fig. 3. First, for a given curve, the ratio κ/α must be less than the peak gain and, as a consequence, α must exceed a minimum threshold value determined by the ratio of κ to the peak gain. Second, the peak gain decreases with Δp_D as a result of Doppler broadening, and this explains why the minimum threshold α of each curve increases with Δp_D. Finally, the threshold value α decreases with Δp_D in the parameter region of sufficiently large positive δ_C. This is because large positive δ_C corresponds to large negative $\delta_L^{(0)}$, where the momentum states of larger Δp_D are more populated than those of smaller Δp_D and consequently require smaller α to create population inversion. Analytical expressions for the threshold values exist for momentum distributions of Lorenzian type, and are presented in Appendix A.

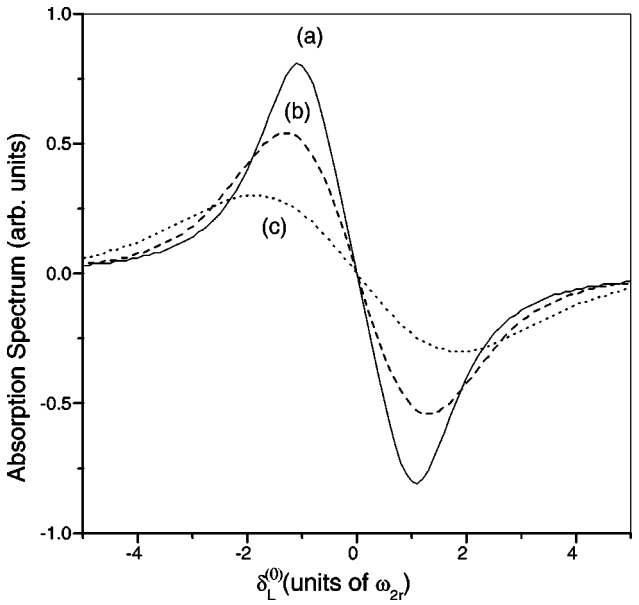

FIG. 3. The absorption spectrum, defined as the left side of Eq. (55), produced with $\gamma_{||}=1$ for (a) the monoenergetic atomic momentum distribution, (b) the Gaussian distribution of $\Delta p_D=0.5$, and (c) the Gaussian distribution of $\Delta p_D=1$.

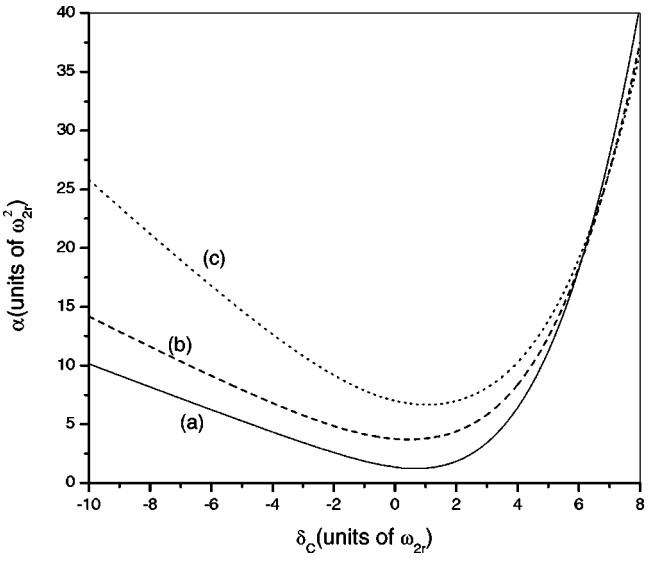

FIG. 4. The lasing or collective instability boundary in the (α,δ_C) parameter space for (a) the monoenergetic atomic momentum distribution, (b) the Gaussian distribution of $\Delta p_D=0.25$, and (c) the Gaussian distribution of $\Delta p_D=0.5$. Additional parameters are $\gamma_{||}=1$ and $\kappa=2$.

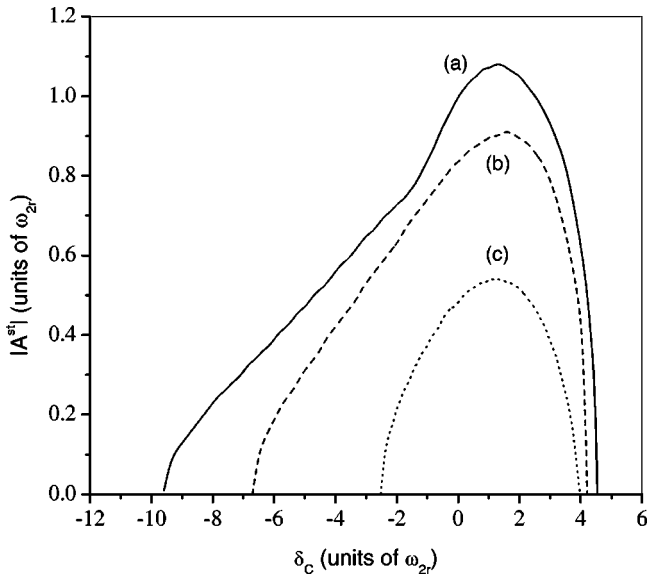

FIG. 5. The steady-state field module $|A^{st}|$ as a function of δ_C for (a) the monoenergetic atomic momentum distribution, (b) the Gaussian distribution of $\Delta p_D = 0.25$, and (c) the Gaussian distribution of $\Delta p_D = 0.5$. Additional parameters are $\gamma_{||} = 1$, $\kappa = 2$, and $\alpha = 10$.

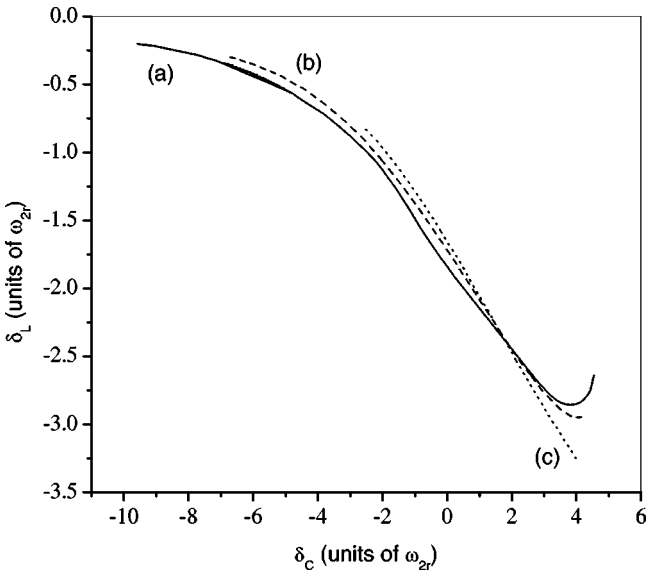

FIG. 6. δ_L as a function of δ_C for (a) the monoenergetic atomic momentum distribution, (b) the Gaussian distribution of $\Delta p_D = 0.25$, and (c) the Gaussian distribution of $\Delta p_D = 0.5$, under the same parameters as in Fig. 5.

B. Stationary steady states

In this subsection, we present and discuss the numerical results performed in the parameter domain where steady states are stationary. In our study below, we will often present examples involving the monoenergetic atomic momentum distribution

$$W(p) = \delta(p), \tag{56}$$

because it models quite well the dynamical behaviors of the CARL system below the subrecoil temperature. The fact that this distribution vanishes everywhere except at $p = 0$ means that we have to consider only a single momentum family $F(p_0 = 0)$, leading to a significant saving in computational time. A distribution like Eq. (56) also means that an arbitrary element in a diffraction group can now be projected onto the basis composed of Dirac-δ functions

$$R_l(p) = \sum_m \Re_l(m)\,\delta(p - m), \tag{57}$$

where m is an integer. This expansion shifts the dynamical variables from $R_l(p)$ to $\Re_l(m)$, whose equations, apart from the pumping term which now becomes $-\gamma_{||}[\Re_l(m) - \delta_{m,0}\delta_{l,0}]$, are the same as those for $R_l(p)$. The field equation also remains the same except that the integration is now substituted by a sum over m: $\Sigma_m \Re_{+1}(m)$.

Consider a system operating at the parameters that give rise to the threshold boundaries of Fig. 4. Figure 5 shows several curves of $|A^{st}|$ as a function of δ_C, each of which is produced by a unique $W(p)$ but under the same condition that $\alpha = 10$. It indicates that for a given Δp_D, the steady-state laser output is indeed bounded between two threshold values δ_C, determined by the intercept of the line $\alpha = 10$ with the curve of the corresponding Δp_D in Fig. 4. Here, $|A^{st}|$ increases gradually with δ_C until it reaches a maximum, beyond which it descends to zero in a rather dramatic fashion, and, for a fixed δ_C, $|A^{st}|$ decreases with increasing Δp_D. Figure 6 displays the corresponding curves of δ_L as a function of δ_C. It shows that the relationship between δ_L and δ_C is quite linear for the situations of large Δp_D but fairly nonlinear for the case of a monoenergetic distribution. The nonlinearity is linked to the fact that the latter maintains a higher steady-state intensity than the former.

To illustrate how the steady state is reached in time, we consider, as an example, the state at the peak of the curve (a) in Fig. 5, where $\delta_C = 1.21$. This state, when calculated by the 2D MCF, is found to have steady-state values of $|A^{st}| = 1.076$ and $\delta_L = -2.21$. The field module $|A|$ as a function of time is shown in Fig. 7(a), indicating that indeed $|A|$ approaches the steady-state value $|A^{st}| = 1.076$, after a short period of oscillations following an initial growth. Periodic structures, implied in Eq. (36), are also evident in both the real and imaginary parts of A at long time, as displayed in Fig. 7(b). The period measured from Fig. 7(b) matches the (angular) frequency shift of $|\delta_L| = 2.21$ at the steady state. Here, the initial growth rate is determined by the real part of the positive eigenvalue governed by Eq. (34). A general trend is that the closer to the threshold points, the slower the initial growth rate, and hence the longer the time delay before arriving at the steady state. In this example, the steady state is approached in oscillations, but it can also be reached monotonically (not shown). It is the interplay between the eigenvalues of the trivial steady state and those of the nontrivial steady state that decides the manner by which the system reaches the steady state.

The growth of the CARL signal is accompanied simultaneously by amplification of the matter waves at different

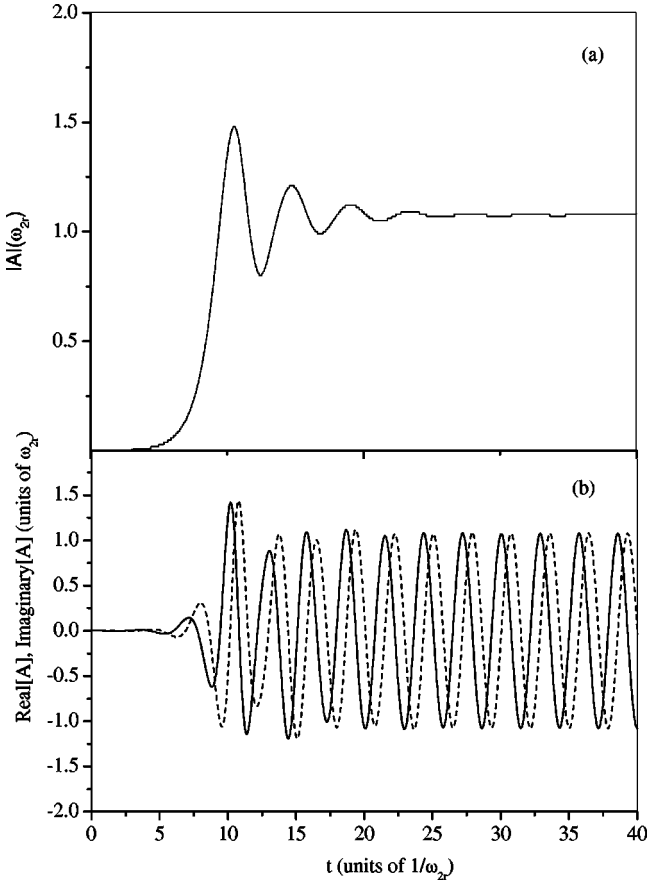

FIG. 7. (a) The field module $|A|$ and (b) the real (solid) and imaginary (dashed) parts of A as a function of time for the monoenergetic momentum distribution. The parameters are $\delta_C=1.21$, $\gamma_{||}=1$, $\kappa=2$, and $\alpha=10$. The initial condition consists of $A=0.001$, and $\Re_l(m)=\delta_{l,0}\delta_{m,0}$.

momentum side modes. It is thus interesting to examine the CARL problem from the perspective of atom optics. For the monoenergetic atomic beam, $R_0(p)=\Sigma_m \Re_0(m)\,\delta(p-m)$, where m can be regarded as the mode number, and the momentum distribution is substituted by the mode distribution function $\Re_0(m)$. Figure 8 represents a distribution of $\Re_0^{st}(m)$ corresponding to the parameters of Fig. 7. It shows that the population, originally all at the mode $m=0$ $[\Re_0(m)=\delta_{m,0}]$, is now being transferred to several momentum side modes. Note that the distribution shows a considerable asymmetry with more modes being excited on the negative than on the positive momentum side. The main signature of the asymmetry is the development of a negative δ_L at which the two-photon resonance is favored for the atoms of negative momenta.

Figure 9 illustrates the time process during which various modes are populated at the expense of the $m=0$ mode. The initial growth rate of each side mode is different. A general trend is that the smaller the mode number $|m|$, the faster the growth rate. The number of modes with significant populations is in proportion to the strength of the CARL signal. This can be explained from the perspective of perturbation theory. The coupling between any two adjacent modes is accomplished via the field amplitude A. As a result, the

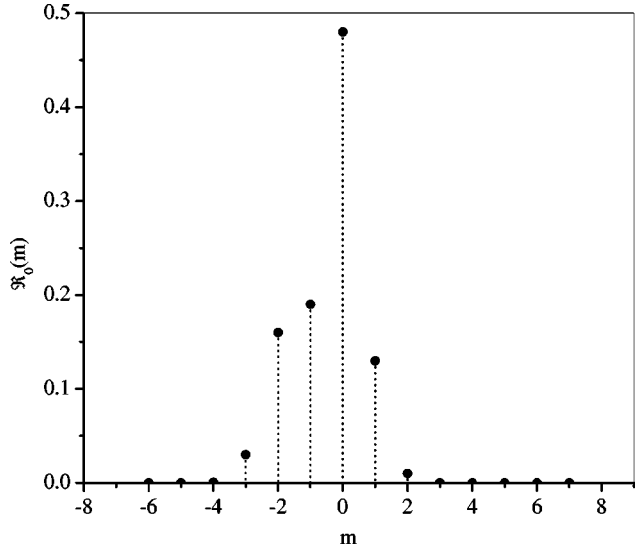

FIG. 8. The distribution of atomic population $\Re_0(m)$ at different momentum modes m under the parameters of Fig. 7.

larger the amplitude A, the more diffraction groups, or equivalently the more modes, are needed in order to produce an accurate description of the system.

The concept of momentum mode is applicable only to momentum distributions of extremely narrow width. Illustrated in Fig. 10 are the steady-state momentum distributions corresponding to $W(p)$ of width (a) $\Delta p_D=0.25$ and (b) $\Delta p_D=0.5$ while the remaining parameters are the same as in Fig. 7. When $\Delta p_D=0.25$, the mode structure, although broadened compared to Fig. 8, is still discernible. This is in contrast to $\Delta p_D=0.5$ where the mode structure is already difficulty to recognize. The fact that a matter wave of very cold atoms can be described by the superposition of different momentum modes lays the foundation for regarding CARL as a parametric wave mixing process involving both optical and atomic waves.

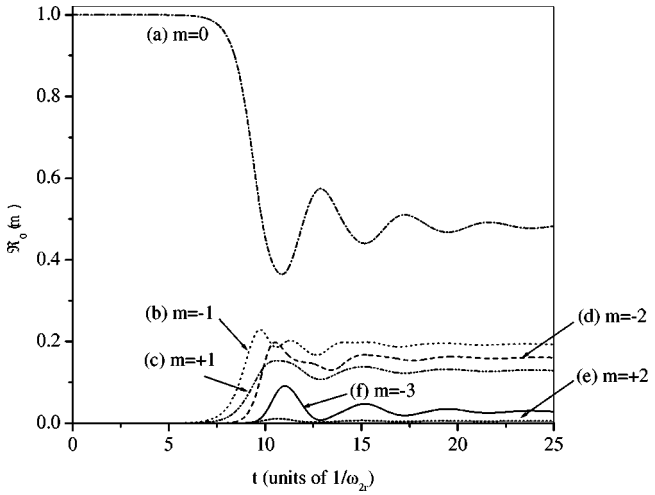

FIG. 9. The time evolution of (a) $\Re_0(0)$, (b) $\Re_0(-1)$, (c) $\Re_0(+1)$, (d) $\Re_0(-2)$, (e) $\Re_0(+2)$, and (f) $\Re_0(-3)$, produced with the parameters of Fig. 7.

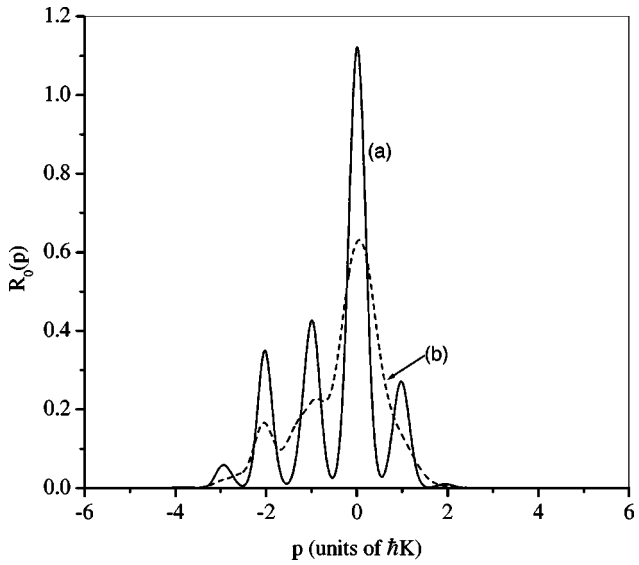

FIG. 10. The steady-state atomic momentum distributions of systems with $W(p)$ of width of (a) $\Delta p_D = 0.25$ and (b) $\Delta p_D = 0.5$. The remaining parameters are the same as those of Fig. 7.

C. Instabilities of steady states

In this subsection, we shift our focus to the parameter space where the steady states are unstable. The linear stability analysis is carried out using the algorithm outlined in Appendix B. It can be shown that, if λ is an eigenvalue of Eqs. (44), (45), and (46), λ^* will also be an eigenvalue of the same equations with its eigenfunctions being the complex conjugates of those for λ. In dealing with such paired eigenvalues, we keep only the eigenvalue with the positive imaginary part without loss of generality. Further, we label the eigenvalues (λ_n, $n=1,2,3,\ldots$) in the sequence of decreasing real parts of the eigenvalues. Note that, since there is always a $\lambda=0$ eigenvalue, $\lambda=0$ will not be part of the sequence for simplicity. Our search for instabilities begins with a stable state corresponding to the point where $\delta_C=0$, on the curve (a) of Fig. 5. The largest four eigenvalues of this state are $\lambda_1=-0.46+1.22i$, $\lambda_2=-0.82+2.23i$, $\lambda_3=-1.08+3.65i$, and $\lambda_4=-1.30+5.22i$, and the time evolution of $|A|$ is depicted in Fig. 11(a).

First, we keep all the parameters the same while gradually increasing α. As α increases, the steady-state intensity increases with α , and, at the same time, it is reached in oscillations of better defined period. An example in which $\alpha=25$ is shown in Fig. 11(b). A well-defined frequency of transitory oscillations is often an indication that the second eigenvalue is much smaller than the first eigenvalue. An examination of the eigenvalues indicates that $\lambda_1=-0.10+2.10i$ is increased, the second and third ones have disappeared, and the fourth one has now become the second one, with the result that $\lambda_2=-1.40+6.62i$ is much smaller than λ_1. Since λ_1 can outlive λ_2 for a long period of time, the fundamental frequency of the transitory oscillations is dominated by the imaginary part of λ_1, which is 2.10, in agreement with the measured frequency from Fig. 11(b).

Note that the real part of λ_1 is already very close to zero when $\alpha=25$. If we continue to increase α, we might be able

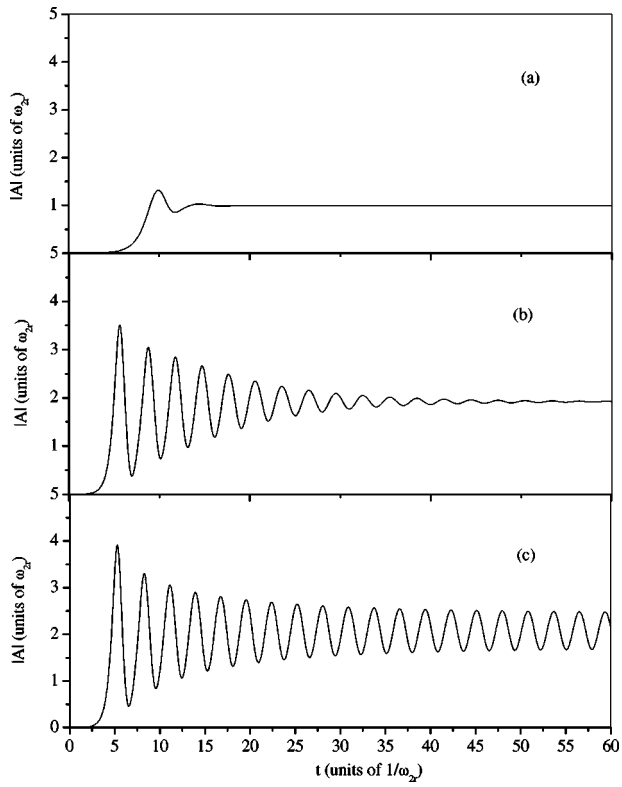

FIG. 11. $|A|$ as a function of time for (a) $\alpha=10$, (b) $\alpha=25$, and (c) $\alpha=28$ with $\delta_C=0$. The remaining parameters along with initial conditions are the same as in Fig. 7.

to change the real part of λ_1 from negative to positive. This turns out to be true. For example, when $\alpha=28$, $\lambda_1=0.02+2.20i$ and $\lambda_2=-1.44+6.89i$. The time evolution of $|A|$ is shown in Fig. 11(c), where the instability is manifest in the form of self-pulsing with a frequency close to 2.20, the imaginary part of λ_1. As α increases further, it seems, for the parameters we tested, that λ_1 continues to be much larger than λ_2 so that there is no competition between the two eigenvalues; the instability continues to exist in the form of self-pulsing but with an increased frequency and amplitude.

Next, we keep all the parameters the same as in Fig. 11(a) while gradually reducing $\gamma_{||}$. As $\gamma_{||}$ decreases, the first four eigenvalues, instead of either vanishing or moving far apart as in the case of increasing α, actually get closer to each other as shown in Fig. 12. This closeness among different eigenvalues is believed to be the cause of the rather irregular transitory development toward the steady state shown in Fig. 13(a) where $\gamma_{||}=0.5$. If $\gamma_{||}$ is reduced to 0.4, $\lambda_1=0.02+0.84i$ becomes positive while the rest are still negative. The time evolution of $|A|$[Fig. 13(b)] displays again a self-pulsing form but with rather distorted cycles. If $\gamma_{||}$ is dropped to 0.3 both $\lambda_1=0.13+0.65i$ and $\lambda_2=0.03+2.5i$ become positive. Under this condition, the self-pulsing structure surprisingly collapses into an extremely irregular form [Fig. 13(c)], reminiscent of the complicated patterns reported by Bonifacio and co-workers [2].It appears, for the parameters tested, that the irregular dynamical pattern persists when $\gamma_{||}$ is below 0.3 (not shown). It is important for atom optics that, because of the coupling between optical and

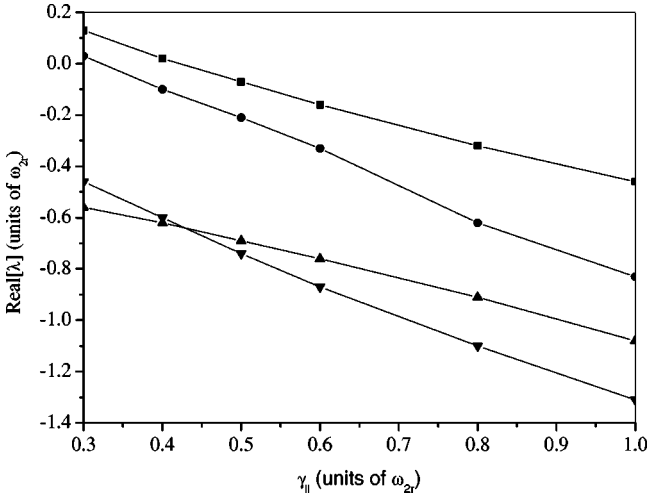

FIG. 12. The real parts of the eigenvalues as functions of $\gamma_{||}$ when $\delta_C=0$. The remaining parameters are same as in Fig. 7.

atomic waves, the matter waves exhibit similar dynamical features as indicated by the time evolution of the population of mode $m=-1$ in Fig. 14. In what follows, we give an estimation of the mean longitudinal speed of sodium atoms corresponding to $\gamma_{||}=0.3$. The unit of $\gamma_{||}$ is ω_{2r}, which is about $4\omega_r$. For sodium atoms, ω_r is about $9.48\times10^4 s^{-1}$.

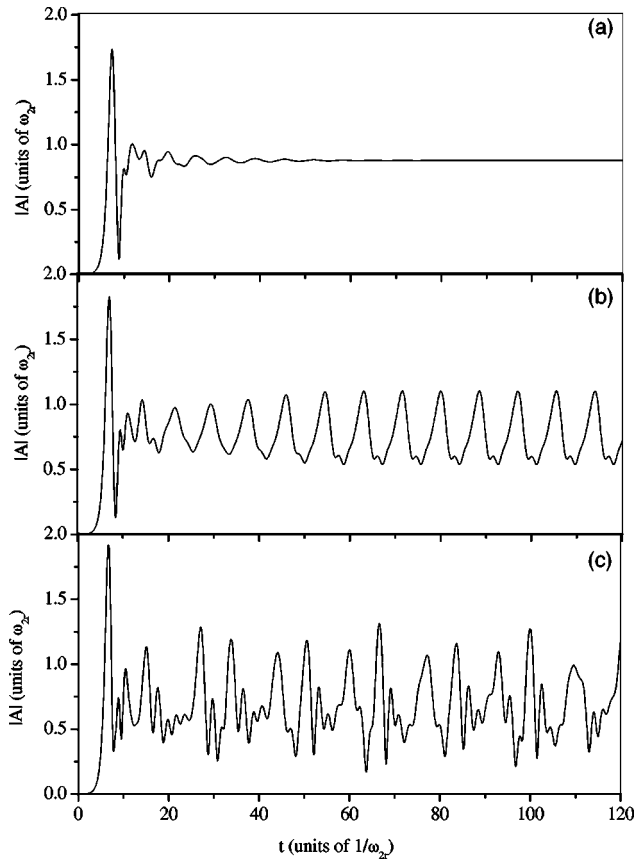

FIG. 13. $|A|$ as a function of time for $\gamma_{||}=0.5$(a), 0.4 (b), and 0.3 (c) with $\delta_C=0$. The remaining parameters along with initial conditions are the same as in Fig. 7.

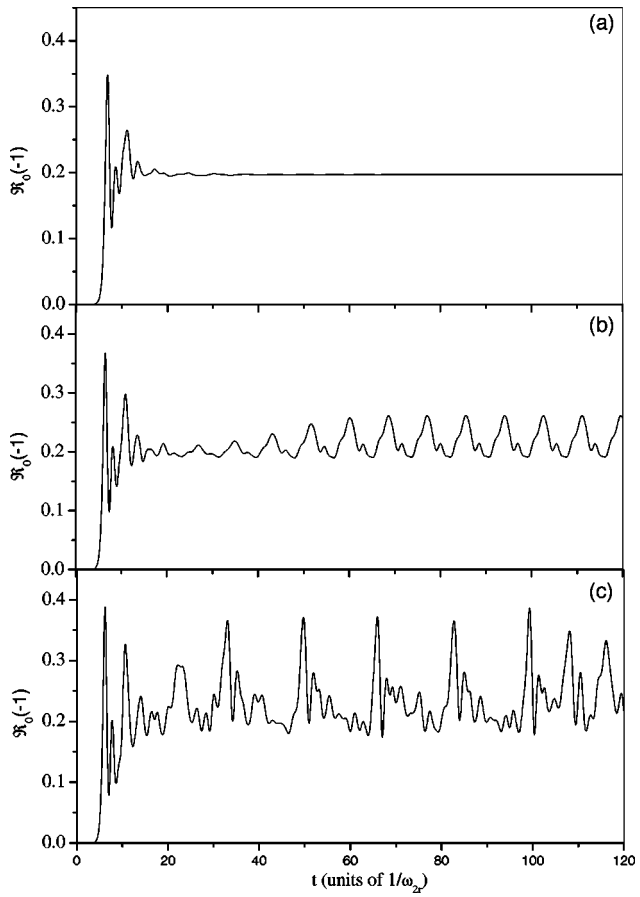

FIG. 14. $\Re_0(-1)$ as a function of time for $\gamma_{||}=0.5$(a), 0.4 (b), and 0.3 (c) with $\delta_C=0$. The remaining parameters and initial conditions are the same as in Fig. 7.

This leads to $\gamma_{||}=1.137\times10^5\,s^{-1}$ or equivalently a transient time of 8.8 μs. If the diameter of the pump field is 10 μm, the mean longitudinal speed will be about 113 cm/s, which is faster than the Doppler limit 30 cm/s, and is, of course, well above the recoil limit 3 cm/s. Since a mean longitudinal speed below 113 cm/s can be obtained by a variety of cooling mechanisms, we conclude that the irregular dynamics is accessible to current experiments.

V. CONCLUSION

In this paper, we formulated a quantum-mechanical CARL theory that treats both internal and external degrees of atomic freedom quantum mechanically but regards laser light as a classical field obeying Maxwell's equations. In forming the theory, we developed an approach in which matter equations were organized in terms of the variables derived from the concepts of momentum families and diffraction groups. This approach has the advantage of transforming the matter equations into forms that allow a straightforward numerical implementation of 2D MCF.

Our 2D MCF seeks to achieve computational efficiency with two layers of reduction of the density matrix elements in momentum space. First, we divide the total momentum space into a limited number of momentum families of smaller space. Next, we divide each family into different

diffraction groups of dimension much smaller than the total number of density matrix elements of a single family. In this way, the matrices to be manipulated in the 2D MCF have dimensions much smaller than the dimension of the total space, leading to tremendous savings in computational time for systems with a large number of momentum side modes.

One of the reasons that the CARL appears different from RIR is that the CARL emphasizes the transient growth while RIR focuses on the amplification at long time. Since our theory covers both time domains, we are likely to unify both theories. Indeed, we found that collective instabilities of CARL develop in the same parameter space where the linear gain of RIR exceeds the cavity loss. This clearly establishes that the gain mechanism of both CARL and RIR has the same origin. In RIR, there is no cavity and the gain is realized by tuning the probe to the red side of the pump. In the CARL, the gain is also achieved by a redshift of the probe relative to the pump (meaning a negative frequency detuning $\delta_L^{(0)}$) except that this redshift is produced dynamically.

In addition to the frequency and amplitude of the CARL signal, we also examined the steady-state distributions of matter waves. Much of the recent enthusiasm about the CARL stems from its applications in atom optics. The CARL can be regarded as a parametric amplifier of coherent matter waves in which the injected mode of the matter wave is converted to the matter waves of side modes. From this point of view, we have in effect presented a study of wave mixing involving many modes of matter waves and two optical waves.

The CARL model is inherently rich and complex in dynamics because, unlike in ordinary laser theory, where the momentum is treated as a dummy variable, the momentum in the CARL becomes a dynamical variable. The number of dynamical variables increases with the number of modes being excited. In this paper, we performed a linear stability analysis of a limited number of nontrivial steady states. We found that instabilities can manifest themselves either in the form of self-pulsings of well-defined period or in the form of irregular pulses. It seems, from our limited experience, that the former occurs when α is sufficiently large while the latter emerges when the transit interaction time is sufficiently long. It is important for atom optics that the matter waves develop similar instabilities. If we operate the CARL in the unstable parameter region, we can create atomic waves whose intensities are modulated in time either periodically or chaotically. These modulated matter waves may find use in future applications.

As a future study, we plan to extend this work to situations where trapped Bose condensates are employed. We also plan to investigate the possibilities of using 2D MCF as a numerical tool for studying the statistical properties of both matter and light waves.

ACKNOWLEDGMENTS

H.Y.L. thanks Professor L. M. Narducci for many useful suggestions during the course of this work, Dr. T. Cai for first introducing him to 2D MCF, and Professor T. R. Vhandrupatla for information about numerical simulation. The work at Rowan was supported by a grant from the Research Corporation.

APPENDIX A: THRESHOLD CONDITION

In this Appendix, we calculate the threshold value α for atomic momentum distributions of Lorenzian type

$$W(p)=\frac{\Delta p_D}{\pi}\frac{1}{p^2+\Delta p_D^2}. \tag{A1}$$

By inserting Eq. (A1) into Eq. (54) and performing contour interactions, we arrive at two relations

$$\kappa+\alpha\gamma_{||}'\frac{4\delta_L^{(0)}}{[\gamma_{||}'^2+(1+\delta_L^{(0)})^2][\gamma_{||}'^2+(1-\delta_L^{(0)})^2]}=0, \tag{A2}$$

$$-\delta_L^{(0)}-\delta_C-\alpha\frac{2\gamma_{||}'^2+2(1-\delta_L^{(0)2})}{[\gamma_{||}'^2+(1+\delta_L^{(0)})^2][\gamma_{||}'^2+(1-\delta_L^{(0)})^2]}=0, \tag{A3}$$

where

$$\gamma_{||}'=\gamma_{||}+2\Delta p_D.$$

By combining Eqs. (A2) and (A3), we find a quadratic equation for $\delta_L^{(0)}$,

$$(\kappa+2\gamma_{||}')\delta_L^{(0)2}+2\gamma_{||}'\delta_C\delta_L^{(0)}-\kappa(1+\gamma_{||}'^2)=0.$$

By solving the quadratic equation, we arrive at

$$\delta_L^{(0)}=\frac{-\gamma_{||}'\delta_C-\sqrt{\gamma_{||}'^2\delta_C^2+\kappa(\kappa+2\gamma_{||}')(1+\gamma_{||}'^2)}}{\kappa+2\gamma_{||}'}, \tag{A4}$$

where we keep only the negative root since Eq. (A2) can be satisfied only when $\delta_L^{(0)}$ is negative. Given a δ_C, we can first determine $\delta_L^{(0)}$ from Eq. (A4), and then insert the $\delta_L^{(0)}$ into either Eq. (A2) or Eq. (A3) to obtain the threshold value α. The curve (a) of Fig. 4 for the monoenergetic atomic beam is calculated using these formulas with $\Delta p_D=0$.

APPENDIX B: LINEAR STABILITY ANALYSIS

In this Appendix, we present a numerical method based upon 2D MCF for obtaining eigenvalues from the linear coupled equations (44), (45), and (46). To begin with, we note that if we can express

$$\int \delta R_{+1}(p)dp=-i\delta AC_{+1}^1-i\delta A^*C_{+1}^2, \tag{B1a}$$

$$\int \delta R_{-1}(p)dp=-i\delta AC_{-1}^1-i\delta A^*C_{-1}^2 \tag{B1b}$$

we can then combine Eqs. (B1) with Eqs. (44) and (45) to form an eigenvalue equation,

$$f(\lambda)=[i(\delta_L+\delta_C)-\kappa-\lambda-\alpha C^1_{+1}]\times[-i(\delta_L+\delta_C)-\kappa-\lambda+\alpha C^2_{-1}]+\alpha^2 C^1_{-1}C^2_{+1}=0,$$

where $C^1_{\pm 1}$ and $C^2_{\pm 1}$ are functions of λ to be determined from Eq. (46). To yield the form of Eqs. (B1), we need to divide each $\delta R_l(p)$ into two components $\delta R^1_l(p)$ and $\delta R^2_l(p)$ according to

$$\delta R_l(p)=-i\,\delta A\,\delta R^1_l(p)-i\,\delta A^*\,\delta R^2_l(p).$$

The equations for $\delta R^1_l(p)$ and $\delta R^2_l(p)$ are found, from Eq. (46), to satisfy, respectively,

$$\begin{aligned}R^{st}_{l-1}(p)-R^{st}_{l-1}(p-1)&=-[il(2p-l-\delta_L)+\lambda+\gamma_{||}]\delta R^1_l(p)+i|A^{st}|\\&\times[\delta R^1_{l+1}(p)-\delta R^1_{l+1}(p+1)]+i|A^{st}|\\&\times[\delta R^1_{l-1}(p)-\delta R^1_{l-1}(p-1)]\end{aligned}\tag{B2}$$

and

$$\begin{aligned}R^{st}_{l+1}(p)-R^{st}_{l+1}(p+1)&=-[il(2p-l-\delta_L)+\lambda+\gamma_{||}]\delta R^2_l(p)+i|A^{st}|\\&\times[\delta R^2_{l+1}(p)-\delta R^2_{l+1}(p+1)]+i|A^{st}|\\&\times[\delta R^2_{l-1}(p)-\delta R^2_{l-1}(p-1)].\end{aligned}\tag{B3}$$

The connection between the two components and all the coefficients is accomplished through the following integrations:

$$C^1_{+1}=\int \delta R^1_{+1}(p)dp,\quad C^2_{+1}=\int \delta R^2_{+1}(p)dp,\tag{B4a}$$

$$C^1_{-1}=\int \delta R^1_{-1}(p)dp,\quad C^2_{-1}=\int \delta R^2_{-1}(p)dp,\tag{B4b}$$

according to Eq. (B1). Both Eq. (B2) and Eq. (B3) show that $\delta R^m_l(p)$, where $m=1$ and 2, are coupled only to the $(l\pm 1)$th diffraction groups and therefore can also be solved by 2D MCF. However, this 2D MCF is more complex than that presented in Sec. III. In the latter case, we can take advantage of Eq. (15) to limit the diffraction groups to $l\geqslant 0$. This is no longer the case here since Eq. (15) does not hold for $\delta R_l(p)$. As a result, we have to treat all the diffraction groups between $-l_{\max}$ and $+l_{\max}$ in a uniform manner. With this in mind, we introduce, for a given momentum family p_0, two vectors $\vec{S}^1_l$ and $\vec{S}^2_l$ of dimension $D(l)=2N_{\max}-|l|+1$. These two vectors are used to hold, respectively, all the elements $\delta R^1_l(p)$ and $\delta R^2_l(p)$ of a given diffraction group l. They are defined as

$$\vec{S}^m_l[n]=\delta R^m_l(p[n]),\ m=1\text{ or }2, n=1,2,\ldots,D(l),\tag{B5}$$

where $p[n]=p_0+(l+|l|)/2+n-N_{\max}-1$. With this definition, we can now cast Eqs. (B2) and (B3) into inhomogeneous tridiagonal matrix forms

$$M_{l,l}\vec{S}^m_l+M^-_{l,l-1}\vec{S}^m_{l-1}+M^+_{l,l+1}\vec{S}^m_{l+1}=\vec{W}^m_l.\tag{B6}$$

$M_{l,l}$ is a diagonal matrix of dimension $D(l)\times D(l)$ and its diagonal elements are defined as

$$M_{l,l}[n][n]=-il(2p[n]-l-\delta_L)-\gamma_{||}-\lambda.$$

$M^+_{l,l+1}$ is a matrix of dimension $D(l)\times D(l+1)$ whose elements are all zero except

$$M^+_{l,l+1}[n][n]=-i|A^{st}|,\ M^+_{l,l+1}[n+1][n]=i|A^{st}|\text{ if }l\geqslant 0,$$

and

$$M^+_{l,l+1}[n][n]=i|A^{st}|,\ M^+_{l,l+1}[n][n+1]=-i|A^{st}|\text{ if }l<0.$$

$M^-_{l,l-1}$ is a matrix of dimension $D(l)\times D(l-1)$ whose elements are all zero except

$$M^-_{l,l-1}[n][n]=-i|A^{st}|,$$

$$M^-_{l,l-1}[n][n+1]=+i|A^{st}|\text{ if }l>0,$$

and

$$M^-_{l,l-1}[n][n]=i|A^{st}|,$$

$$M^-_{l,l-1}[n+1][n]=-i|A^{st}|\text{ if }l\leqslant 0.$$

Finally, $\vec{W}^m_l$ are vectors of dimension $D(l)$ defined as

$$\vec{W}^1_l[n]=R^{st}_{l-1}(p[n])-R^{st}_{l-1}(p[n]-1),$$

$$\vec{W}^2_l[n]=R^{st}_{l+1}(p[n])-R^{st}_{l+1}(p[n]+1).$$

To solve Eq. (B6), we introduce a forward ansatz,

$$\vec{S}^m_l=-Q^{m+}_l M^-_{l,l-1}\vec{S}^m_{l-1}+\vec{C}^m_l,\tag{B7}$$

where Q^{m+}_l is a matrix of dimension $D(l)\times D(l)$, and $\vec{C}^m_l$ is a vector of dimension $D(l)$, both of which are unknown. Replacing $\vec{S}^m_{l+1}$ in Eq. (B6) with Eq. (B7) for $l=l+1$, and comparing the result with Eq. (B7), we find the following recursive relations:

$$Q^{m+}_l=(M_{l,l}-M^+_{l,l+1}Q^{m+}_{l+1}M^-_{l+1,l})^{-1},\tag{B8a}$$

$$\vec{C}^m_l=Q^{m+}_l(\vec{W}^m_l-M^+_{l,l+1}\vec{C}^m_{l+1}).\tag{B8b}$$

The starting values for the recursive relations are determined by the boundary condition that $\vec{S}^m_{l_{\max}+1}=\vec{0}$. By inserting $\vec{S}^m_{l_{\max}+1}=\vec{0}$ into Eq. (B6) for $l=l_{\max}$ and comparing the result with Eq. (B7), we find that

$$Q^{m+}_{l_{\max}}=(M^m_{l_{\max},l_{\max}})^{-1},\tag{B9a}$$

$$\vec{C}^m_{l_{\max}} = Q^{m+}_{l_{\max}} \vec{W}^m_{l_{\max}}. \tag{B9b}$$

As a result, all the matrices Q^{m+}_l and the vectors $\vec{C}^m_l$ with $l < l_{\max}$ can be obtained from Eqs. (B8) recursively, starting from Eqs. (B9).Finally, all the vectors $\vec{S}^m_l$ with $l > l_{\min}$ can be derived according to Eq. (B7) in a forward substitution, starting from

$$\vec{S}^m_{l_{\min}} = \frac{\vec{W}^m_{l_{\min}} - M^+_{l_{\min},l_{\min}+1}\vec{C}^m_{l_{\min}+1}}{M_{l_{\min},l_{\min}} - M^+_{l_{\min},l_{\min}+1}Q^{m+}_{l_{\min}+1}M^-_{l_{\min}+1,l_{\min}}},$$

which is obtained by simultaneously solving Eq. (B7) with $l = l_{\min}+1$ and Eq. (B6) for $l = l_{\min}$, keeping in mind the boundary condition $\vec{S}^m_{l_{\min}-1} = \vec{0}$. By repeating the steps for each momentum family, we can construct $\delta R^1_{\pm 1}(p)$ and $\delta R^2_{\pm 1}(p)$, which are used to construct $C^1_{\pm 1}$ and $C^2_{\pm 1}$.

[1] R. Bonifacio and L. De Salvo, Nucl. Instrum. Methods Phys. Res. A **341**, 360 (1994).
[2] R. Bonifacio, L. De Salvo, L. M. Narducci, and E. J. D'Angelo, Phys. Rev. A **50**, 1716 (1994).
[3] R. Bonifacio and L. De Salvo, Appl. Phys. B: Lasers Opt. **60**, 233 (1995).
[4] L. De Salvo, R. Cannerozzi, R. Bonifacio, E. J. D'Angelo, and L. Narducci, Phys. Rev. A **52**, 2342 (1995).
[5] R. Bonifacio, G. R. M. Robb, and B. W. J. McNeil, Phys. Rev. A **56**, 912 (1997).
[6] G. L. Lippi, G. P. Barozzi, S. Barbay, and J. R. Tredicce, Phys. Rev. Lett. **76**, 2452 (1996).
[7] P. R. Hemmer, N. P. Bigelow, D. P. Katz, M. S. Shahriar, L. De Salvo, and R. Bonifacio, Phys. Rev. Lett. **77**, 1468 (1996).
[8] W. J. Brown, J. R. Gardner, D. J. Gauthier, and R. Vilaseca, Phys. Rev. A **55**, R1601 (1997).
[9] J. Guo, P. R. Berman, B. Dubetsky, and G. Grynberg, Phys. Rev. A **46**, 1426 (1992).
[10] J. Guo and P. R. Berman, Phys. Rev. A **47**, 4128 (1993).
[11] J.-Y. Courtois, G. Grynberg, B. Lounis, and P. Verkerk, Phys. Rev. Lett. **72**, 3017 (1994).
[12] P. R. Berman, Phys. Rev. A **59**, 585 (1999).
[13] M. G. Moore and P. Meystre, Phys. Rev. A **58**, 3248 (1998).
[14] S. Haroche and F. Hartmann, Phys. Rev. A **6**, 1280 (1972).
[15] S. Stenholm, Appl. Phys. **15**, 287 (1978).
[16] G. Lenz, P. Meystre, and E. M. Wright, Phys. Rev. Lett. **71**, 3271 (1993).
[17] W. Zhang, D. F. Walls, and B. C. Sanders, Phys. Rev. Lett. **72**, 60 (1994).
[18] J. Stenger, S. Inouye, D. M. Stamper-Kurn, H. J. Meisner, A. P. Chikkatur, and W. Ketterle, Nature (London) **396**, 345 (1998).
[19] L. Deng, E. W. Hagley, J. Wen, M. Trippenbach, Y. Band, P. S. Julienne, J. E. Simsarian, K. Helmerson, S. L. Roston, and W. D. Phillips, Nature (London) **398**, 218 (1999).
[20] S. Inouye, A. P. Chikkatur, D. M. Stamper-Kurn, J. Stenger, D. E. Pritchard, and W. Ketterle, Science **285**, 571 (1999).
[21] M. G. Moore and P. Meystre, Phys. Rev. Lett. **83**, 5202 (1999).
[22] C. K. Law and N. P. Bigelow, Phys. Rev. A **58**, 4791 (1998).
[23] M. G. Moore and P. Meystre, Phys. Rev. A **59**, R1754 (1999); M. G. Moore, O. Zobay, and P. Meystre, *ibid.* **60**, 1491 (1999).
[24] H. Zeng, W. Zhang, and F. Lin, Phys. Rev. A **52**, 455 (1995).
[25] C. J. Bordè, in *Advances in Laser Spectroscopy*, edited by F. S. T. Arrechi and H. Walther (Plenum Press, New York, 1983).
[26] Y. Castin, H. Wallis, and J. Dalibard, J. Opt. Soc. Am. B **6**, 2046 (1989).
[27] A. Aspect, E. Arimondo, R. Kaiser, N. Vansteenkiste, and C. Cohen-Tannoudji, J. Opt. Soc. Am. B **6**, 2112 (1989).
[28] T. Cai, H. Pu, and N. P. Bigelow, in *Coherence and Quantum Optics VII*, edited by J. H. Eberly, L. Mandel, and E. Wolf (Plenum Press, New York, 1996), p. 379.
[29] H. Pu, T. Cai, and N. P. Bigelow, Eur. Phys. J. D **7**, 269 (1999).
[30] H. Y. Ling, Phys. Rev. A **59**, 3714 (1999).
[31] H. Y. Ling and A. Williams, Phys. Rev. A **60**, 4812 (1999).
[32] L. Narducci and N. Abraham, *Laser Physics and Laser Instabilities* (World Scientific, Teaneck, NJ, 1988).
[33] M. Sargent III, M. Scully, and W. E. Lamb, Jr., *Laser Physics* (Addison-Wesley, New York, 1994).
[34] W. H. Press, B. P. Flannery, S. A. Teukolsky, and W. T. Vetterling, *Numerical Recipes in C* (Cambridge University Press, New York, 1988).
[35] A. D. Belegundu and T. R. Chandrupatla, *Optimization Concepts and Applications in Engineering* (Prentice-Hall, Englewood Cliffs, NJ, 1999).